Internal architecture of coffin-shaped ZSM-5 zeolite crystals with hourglass contrast unravelled by focused ion beam-assisted transmission electron microscopy

Lay Description

Understanding the internal structure, such as defects, boundaries, crystallographic orientations and intergrowth, of crystallites is essential for improving their performance. Meanwhile, three-dimensional (3D) visualization of internal architecture can also provide much more information than the two-dimensional (2D) image and plays an important role in the improvement of sample fabrication and the explanation of properties. An approach combining focused ion beam and transmission electron microscopy is used to study specific interfaces and internal architecture of the bulk sample and the catalytic crystallites. Several specific lamellas can be fabricated from the different positions of the crystal with the so-called “lift out” technique. TEM observations of these lamellas can provide high resolution information of the microstructure features. The three-dimensional (3D) morphology of the internal architecture can also be built.

Internal architecture of coffin-shaped ZSM-5 zeolite crystals with hourglass contrast unraveled by focused ion beam-assisted transmission electron microscopy

Jiangbo Lu[1,2], Evelyne Bartholomeeusen[3], Bert F. Sels[3], Dominique Schryvers[2*]

[1] School of Electronic and Information Engineering, Xi'an Jiaotong University, Xi'an 710049, People's Republic of China

[2] EMAT, University of Antwerp, Groenenborgerlaan 171, B-2020 Antwerp, Belgium

[3] COK, KU Leuven, Kasteelpark Arenberg 23, B-3001 Heverlee, Belgium

Corresponding author: D. Schryvers

Email: nick.schryvers@uantwerpen.be

Tel: +3232653247

Fax: +32 32653318

Summary

Optical microscopy, focused ion beam and transmission electron microscopy are combined to study the internal architecture in a coffin-shaped ZSM-5 crystal showing an hourglass contrast in optical microscopy. Based on parallel lamellas from different positions in the crystal, the orientation relationships between the intergrowth components of the crystal are studied and the internal architecture and growth mechanism are illustrated. The crystal is found to contain two pyramid-like components aside from a central component. Both pyramid-like components are rotated by 90° along the common c-axis and with respect to the central component while the interfaces between the components show local zigzag feature, the latter indicating variations in relative growth velocity of the two components. The pyramid-like intergrowth components are larger and come closer to one another in the middle of the crystal than at the edges, but they do not connect. A model of multi-site nucleation and growth of 90° intergrowth components is proposed.

Key words: Internal architecture, intergrowth, rotational boundary, ZSM-5, focused ion beam, transmission electron microscopy.

Introduction

In catalysis, zeolites are of great scientific and technological importance as they are widely used in modern chemical industry, such as crude oil refining and ethylbenzene synthesis to facilitate the reaction processes. The crystalline microporous nature of many of these molecular sieves provides them with a unique combination of a high catalytic activity and shape selectivity towards the required end products. As a leading shape selective catalyst in the synthesis of dimethylbenzene (Den Hollander *et al.*, 2002, Wu & Anthony, 1999), ZSM-5 crystals possessing the MFI (mordenite framework inverted)-type micro-porous structure have drawn much attention to scientists worldwide. The MFI-type structure is based on an orthorhombic crystal lattice with a Pnma space group and lattice parameters a=2.0108nm, b=1.9918nm and c=1.3392nm. This structure contains straight channels (5.6×5.3Å^2 in cross-section) along the crystallographic b-axis that are interconnected with sinusoidal channels (5.5×5.1Å^2 in cross-section) along the a-axis. These channels control the transport of reagents and products and induce shape selectivity. In the ideal case, easy diffusion of reactant molecules to the crystals interior is mainly realized in the straight channels running from one large (010) surface to the opposite one. In a similar way the sinusoidal channels run between the smaller (100) outer surfaces of the crystal. However, the large micrometer-sized crystals, especially of the coffin-shaped type, rarely occur as perfect single crystals. Prominent features such as small ramps on the (100) (or occasionally the (010)) faces and more pronounced intergrowths with well-developed morphologies are often observed in electron micrographs or by other techniques including optical microscopy, fluorescence microscopy, electron backscatter diffraction, focused ion

beam and second-harmonic generation microscopy (Stavitski *et al.*, 2008, Karwacki *et al.*, 2007, Van der Veen *et al.*, 2010, Stavitski *et al.*, 2007, Karwacki *et al.*, 2009, Roeffaers *et al.*, 2008a, Roeffaers *et al.*, 2008b, Roeffaers *et al.*, 2007). Already in the early electron microscopic studies by Price et al., the morphology of ZSM-5 crystals is described to contain components in the crystallite which are rotated around a common c-axis by 90 degrees ("twinned" zeolite) (Price *et al.*, 1982). Optical microscopy revealed the 90 degree intergrowth as an hourglass pattern, suggesting it was resulting from a point or small region near the center of the crystal. The way in which building blocks are interconnected and the corresponding internal interfaces may severely influence the intracrystalline molecular transport through the zeolite material or even make certain parts of the zeolite intergrowth components completely inaccessible to the reactant molecules (Karwacki *et al.*, 2009, Roeffaers *et al.*, 2007). Several groups have contributed to the elucidation of crystal intergrowth structures and molecular diffusion barriers. However, in all its complexity, several models, growth mechanisms and explanations for twinning are proposed, whereas giving valuable information, unfortunately, they do not allow for a direct and detailed observation of the intergrowth boundary and internal architecture.

Understanding the internal structure of ZSM-5 crystallites is essential for improving catalyst performance. In order to maximize the performance of ZSM-5 catalysts and to get a complete picture of the catalytic properties and microstructure-function relationships of this material, it is crucial to obtain fundamental knowledge on their internal architecture and boundaries. In the present study, an approach combining optical microscopy, focused ion beam (FIB) and transmission electron microscopy

(TEM) which provides site-specific direct observation of boundary, crystallographic orientations and microstructure features in bulk samples is employed to investigate the intergrowth and internal architecture in coffin-shaped ZSM-5 crystals.

Experimental

Sample Preparation

The zeolite sample was prepared according to method (III) from the paper of Mueller and Unger, with a gel composition of 8TPABr/123$(NH_4)_2O$/Al_2O_3/1400SiO_2/2280 H_2O and with crystallization for 7 days at 180°C (Mueller & Unger, 1988).

The cross-section FIB lamellas were prepared with the so-called “lift out” technique using an FEI Helios NanoLab 650 FIB/SEM dual-beam system. In all cases, an ion-beam-assisted (30KV) protective Pt layer was deposited on the surface of the crystal before FIB cutting. Ga^+ ion beams of 30KV/3nA and 30KV/0.24nA were used for sample cutting and early stage milling. In the final stage, the Ga^+ beam was reduced to 5KV/14pA to minimize the ion beam damage during final milling. In order to directly observe the boundaries between intergrowth components with scanning electron microscopy (SEM), the crystals were etched in 4 vol% HF (295K,15-40s) and subsequently rinsed in methanol (Lu *et al.*, 2014).

Transmission Electron Microscopy

Conventional bright field (BF) TEM and high resolution (HR)TEM were used to observe the intergrowth boundaries and internal architecture after FIB milling, while selected area electron diffraction (SAED) was used to study the orientation relationships between

different components. The optical microscopy observations were carried out on a Leica DMI5000M microscope. The TEM and high-angle annular dark field scanning transmission electron microscopy (HAADF-STEM) observations were performed on an FEI Tecnai microscope operated at 80-200KV. Since the ZSM-5 sample is sensitive to the electron beam, the HRTEM observation was operated at 80 KV in order to reduce electron beam damage. Unfortunately, this implies that the image resolution is somewhat limited. Also, the samples were introduced in the TEM vacuum 8-12 hours before the observations in order to allow for a maximum evaporation of any residual water molecules. Indeed, the latter are known to enhance structural damage in zeolites when being heated by the electron beam.

Results and discussion

As previously stated, the way in which intergrowth structures are interconnected may severely influence the intracrystalline molecular transport through the zeolite material. Internal intergrowth boundaries can act as molecular diffusion barriers inside zeolites have a large impact on their catalytic behavior (Kox *et al.*, 2007, Karwacki *et al.*, 2007, Tzoulaki *et al.*, 2008, Stavitski *et al.*, 2007, Roeffaers *et al.*, 2007, Roeffaers *et al.*, 2008b) Therefore, obtaining detailed information on the internal architecture of the crystalline zeolite and the intergrowth boundaries in particular, is an essential aspect to obtain insight in the performance of the catalysts Figure 1(a) shows a typical optical microscopy image of a coffin-shaped ZSM-5 crystal with dimensions 80*20*13.5 mm^3 revealing an hourglass-like contrast over the full length of the crystal. Figure 1(b) shows the corresponding SEM image of the identical crystal. In order to study the optically

visualized hourglass boundary and internal architecture of the crystal, three parallel FIB lamellas A-B-C from different positions in the crystal have been prepared. The lamellas are indicated by white bars in Figure 1(b), with lamella A being obtained from the middle and lamellas B and C at similar distances on either side of the coffin shaped crystal. The thickness of the FIB lamellas is estimated at 2 microns and finally thinned to around 50 nm.

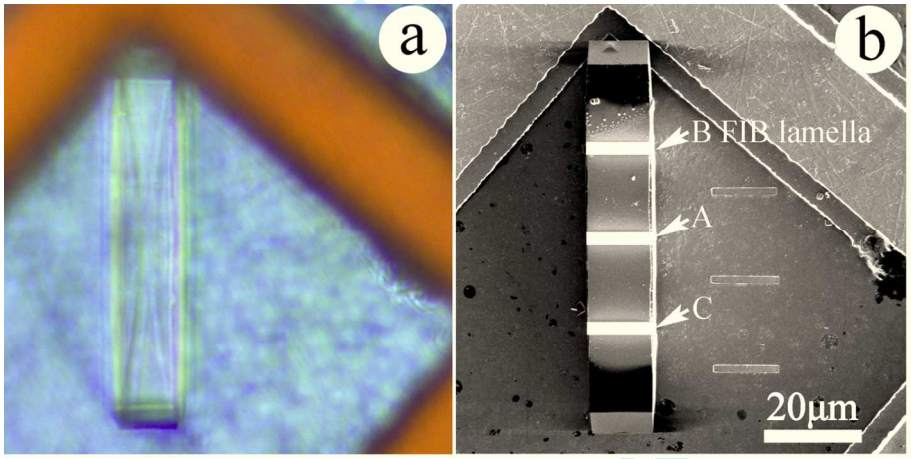

Figure 1. (a) Optical microscopy image of a coffin-shaped ZSM-5 crystal showing an hourglass pattern. (b) SEM image of the same crystal with indications of the sites for FIB sample selection.

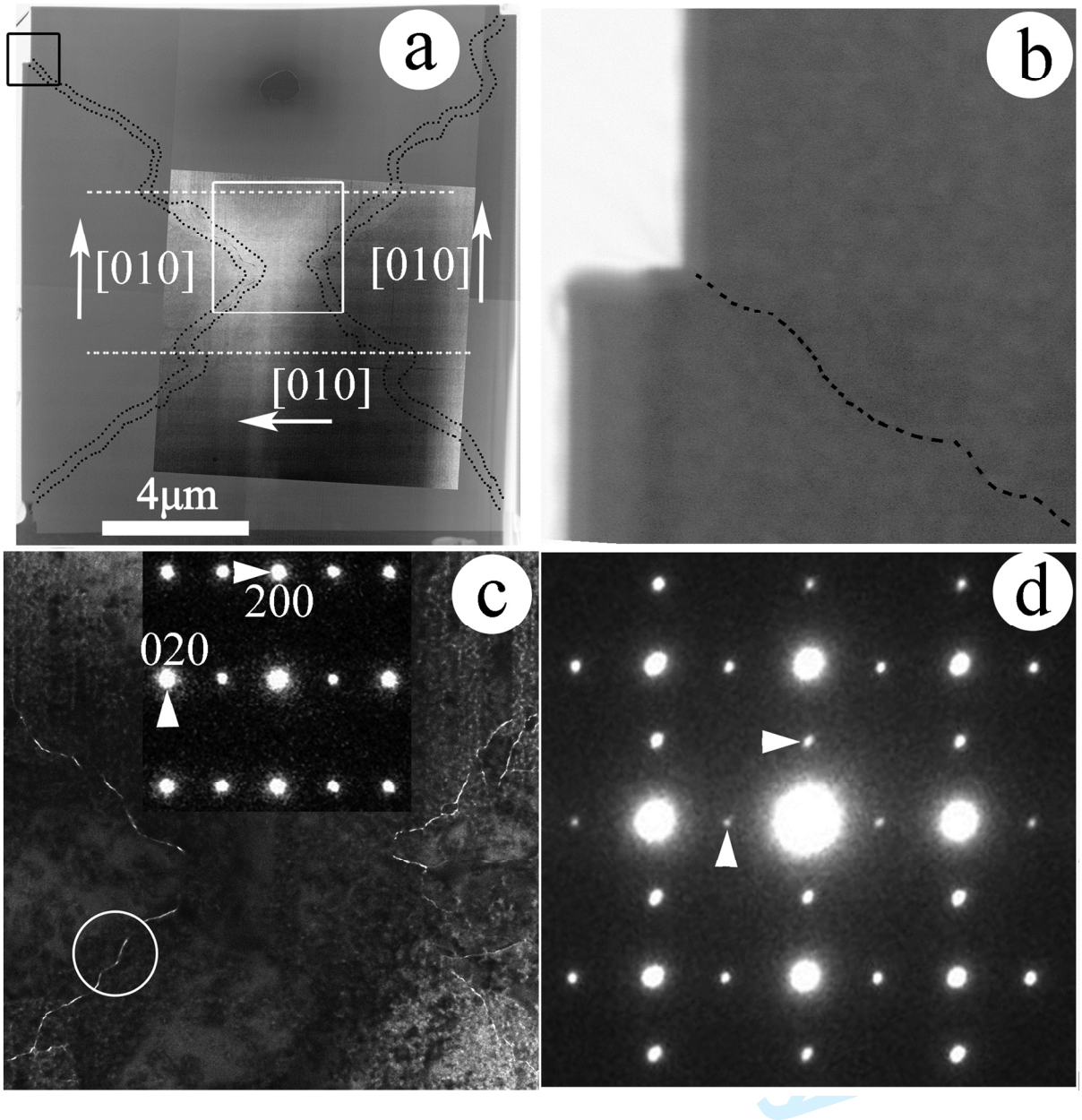

Figure 2. (a) Low magnification STEM image of lamella A. (b) Enlarged image from the black rectangle enclosed region at the upper left corner of (a). (c) Bright field (BF) image of the white square enclosed region in (a) with SAED pattern of the middle part. (d) [001] zone axis SAED pattern from the white circle enclosed boundary region in (a).

Figure 2(a) shows a composite low magnification STEM image of lamella A, composed of several smaller STEM images to give an overview of the whole lamella. The paired dotted lines indicate traces of boundaries between different components. The actual boundary is located in between the paired dotted lines. Figure 2(b) shows an enlarged image of the step on the left corner of the lamella where the dash line indicates the boundary between components and starting at this corner. Figure 2(c) shows a bright field (BF) image from the white squared region in the central part of lamella A in Figure 2(a), indicating the local zigzag feature of the boundaries. Due to the FIB thinning the weaker bonds at the interface have been destroyed yielding voids visible as white lines. The inset in Figure 2(c) shows an SAED pattern form the middle component, indicating the crystallographic orientation of the component, which has also been added to the composed image of Figure 2(a). Figure 2(d) represents the corresponding diffraction pattern from the interface region enclosed by the white circle in Figure 2(c), illustrating the perfect 90° rotational orientation relationship between the two components at each side of the boundary (Figure S1 of the supplementary information shows the same relation for the other side of the crystal). The small difference between the a and b lattice parameters yields a spot splitting only visible far away from the center of the pattern. From high magnification TEM images with unit cell scale resolution it was concluded that the local zigzag curvatures of such 90° rotational boundaries can be resolved as a series of alternating steps of (100)//(010)' and (010)//(100)' with indicating the indexing in the adjacent component (Lu *et al.*, 2014). Millward *et al.* and Hay *et al.* proposed that the number of bonds that oxygen linked between two 90° rotational intergrowths is half that in the ZSM-5 matrix (Millward *et al.*,

1983, Hay *et al.*, 1990), confirming the explanation of the formation of voids at the interfaces.

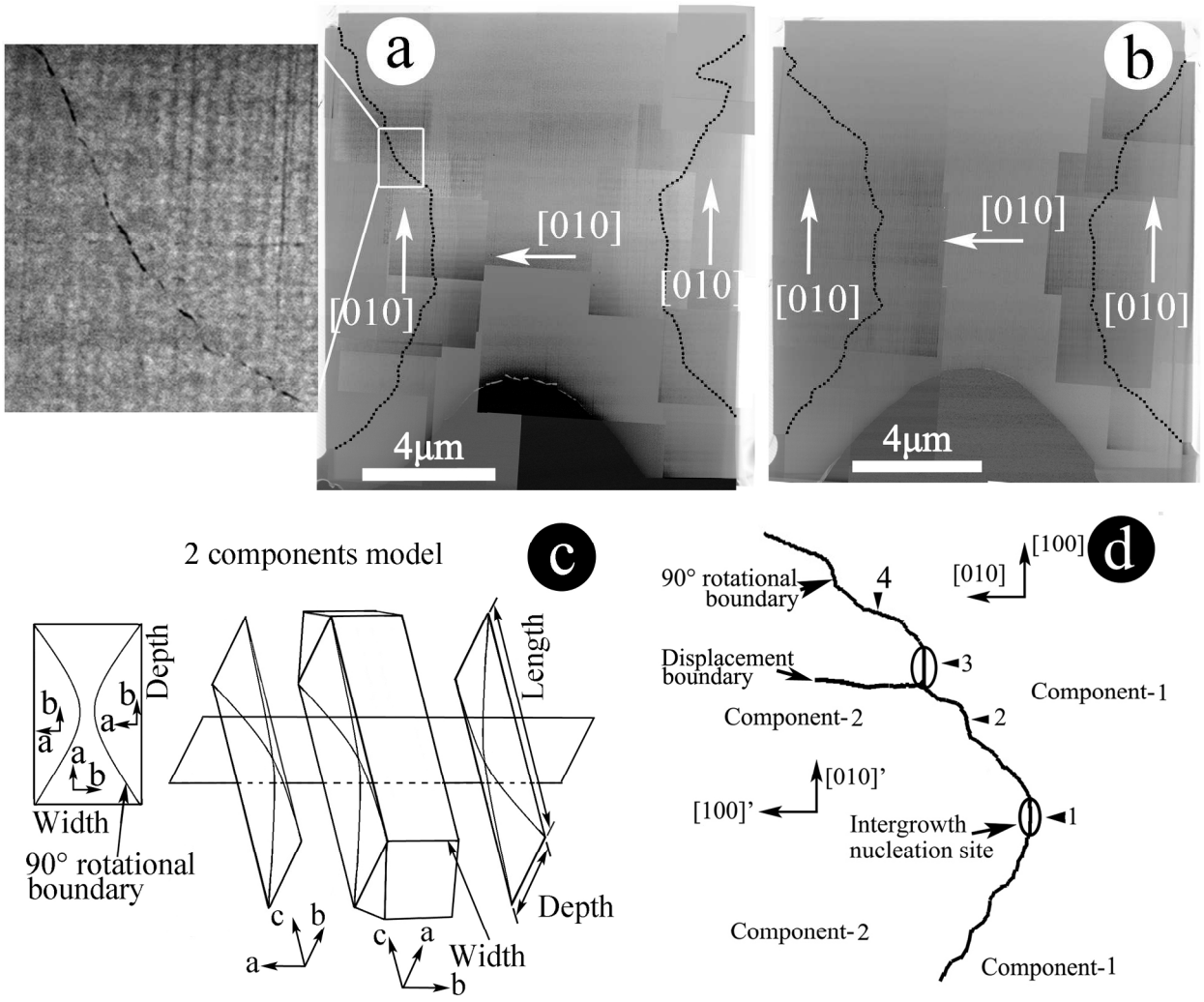

Figure 3. (a) Low magnification STEM image of lamella B. (b) Low magnification STEM image of lamella C. (c) Proposed 2-component model. (d) Proposed model of the multi-site nucleation and growth of 90° intergrowth components.

Figure 3(a) shows a composite low magnification STEM image of lamella B, made up of several smaller STEM images to give an overview of the whole lamella. The

enlargement on the left shows the trace of the intergrowth boundary, which shows some voids again due to the FIB thinning. Figure 3(b) shows a low magnification STEM image of lamella C. The boundaries between different intergrowth components in both Figure 3(a) and 3(b) are indicated by black dotted lines. The arrows indicating the [010] orientations of each component were obtained from the corresponding SAED patterns, as in Figure 2 and confirming the latter (SAED patterns of all components are shown in Figure S2 of the supplementary information).

In earlier studies focusing on the internal intergrowth, 2-component and 3-component models were proposed (Roeffaers *et al.*, 2008a, Roeffaers *et al.*, 2007). In the idealized 2-component model the crystal contains, besides a main component, two pyramidal components connected in the center and which are rotated by 90° around the common c-axis, which corresponds with the long axis of the crystal. Based on our observation in lamella A cut from the central of the crystal and viewed along the long c axis (Figure 2(a)), the present coffin-shaped crystal indeed contains two pyramid-like components besides the main central component. Both components on opposite sides are rotated by 90° around the common c-axis and with respect to the central component, confirming the 2-component model. In reality, however, the interfaces between adjacent components are not straight but reveal local zigzag features. Moreover, the pyramid-like intergrowth components do not make contact in the middle of the lamella, which implies that the main component is continuous in the center and over the length of the crystal. As a result, the sinusoidal channels between opposite (100) faces of the main component can still be continuous over the entire depth of the crystal (cfr. left most cross-section in Figure 3(c)).

Figure 3(d) shows our proposed model of multi-site nucleation and growth of 90° intergrowth components projected along the [001] orientation. The ellipses 1 and 3 show sites where 90° grains can nucleate. When different subgrains join, a displacement boundary may occur. Finally, the different nucleated subgrains connect into one large 90° intergrown component containing several displacement boundaries, as seen before (Lu *et al.*, 2014). According to the sector boundary growth theory of crystal growth in aqueous and organic solutions, the rotational or 90° boundary appears as a straight or somewhat curved line, the local direction of which depends on the (instantaneous) relative growth velocity *v1* and *v2* of these faces (planes). If *v1*/*v2* is constant, the boundary lines are straight (i.e., the boundary is planar); if *v1*/*v2* fluctuates, the lines are irregular, often zigzag-like (i.e., the boundary is an irregularly waved internal surface) (Klapper, 2010). This means that the actual interface geometry simply depends on the relative growth velocity on the two faces. Thus, it can be concluded that at position 2 the growth of component-2 along [010]' is faster than component-1along [010], while at position 4 the growth of component-2 along [010]' is slower than component-1 along [010]. Since the rotational boundaries in our sample are with local zigzag features, we can conclude that the local growth velocities of the components separated by the 90° boundaries fluctuate during growth. The factors that affect the growth velocities of different planes can be the local chemical solution, additive ion concentrations, temperature and mixing procedure of the reagents etc. (Iwasaki *et al.*, 1995, Iwasaki *et al.*, 1998). For aggregated crystals, it is also reported that inter-particle disturbance affects the growth of crystals due to exhaustion of chemical species in the vicinity of the surface (Iwasaki *et al.*, 1995). It can be expected that such a fluctuation of

local growth velocities is a common feature so that zig-zag shapes in 90° intergrowth boundaries as well as displacement boundaries can also occur in other crystals. The resulting displacement boundaries can partially impede the connectivity of the straight channels, thus it can be expected that the catalytic behavior of the crystal can be hindered by the formation of such displacement boundaries inside the crystals. Moreover, since the straight channels run along the [010] direction of the crystal, it can be expected that the 90° rotational boundaries can completely block the connectivity of the straight channels and thus diminish the catalytic behavior of the crystal as also noted by Karwacki *et al.* who indicated that these 90° intergrowth structures in MFI-type crystals can lead to distinct internal molecular diffusion barriers (Karwacki *et al.*, 2009). Since the aspect ratio of our crystals is above 4, we did not observe the small-angle defect planes found by Karwacki *et al.*, nor did we observe any planes with higher defect concentrations connected with the corners of the (101) and (100) faces.

Recently, the intergrowth structure and aluminum zoning in a ZSM-5 crystal were studied by synchrotron-based micro X-ray diffraction imaging (Ristanović *et al.*, 2013). An expansion of the lattice parameters from the middle of the crystal towards the surface was attributed to differences in concentration of aluminum. Such a small lattice parameter expansion was not observed in our sample, which could be due to the limitation of the precision for lattice parameter measurements by TEM. Also, as for the aluminum zone, since the ZSM-5 crystals are very sensitive to the electron beam (even when operated at 80KV), accurate microscopic elemental concentration analysis with energy dispersive X-ray spectroscopy (EDS) or electron energy loss spectroscopy (EELS) cannot be conducted without damaging the sample, thus no elementary

concentration information was obtained in the present experiments. However, if we take a closer look at the morphology (e.g., curvature) of the two 90° intergrowth boundaries in Figure 2(a), which is the cross-section image in the middle of the ZSM-5 crystal, it is noted that the curvatures of the two 90° intergrowth boundaries change abruptly almost at the same distance from the center (as indicated by two dashed horizontal white lines), i.e., at the same time during growth, which may imply a growth velocity change when the crystal grows to a specific size. As discussed before, the factors that affect the growth velocities of different planes can be the local chemical solution, additive ion concentrations etc., so this observation could be in line with a concentration change in the center of the ZSM-5 crystal and which induced the lattice parameter expansion as reported by Ristanović *et al.*

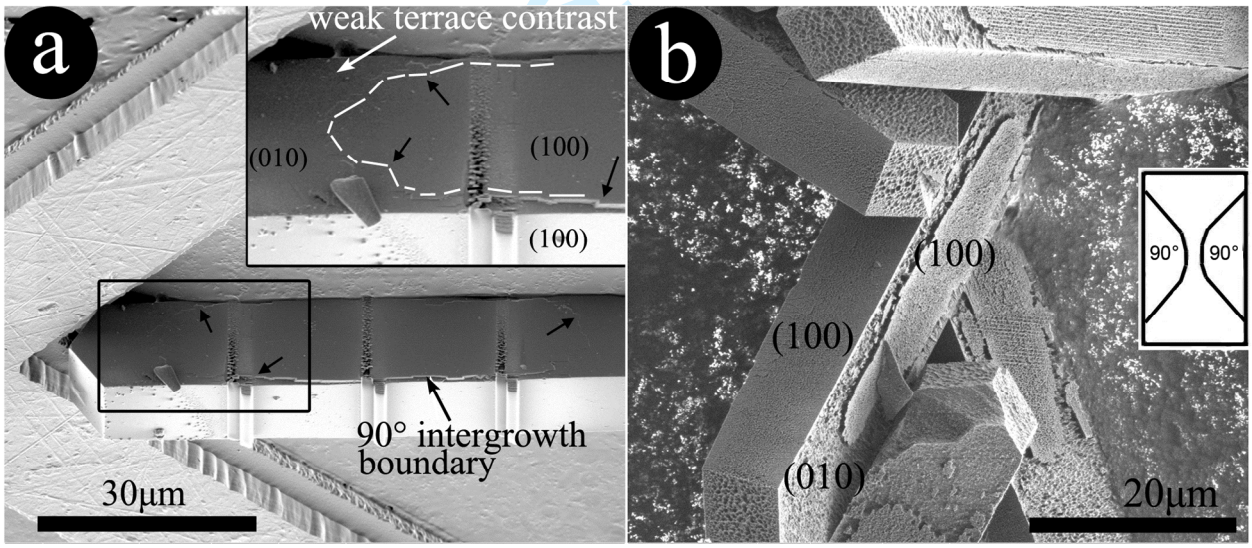

Figure 4. (a) SEM image of the side surface of the crystal in Figure 1: the boundary between the central matrix and the 90° intergrowth is indicated by black arrows and a parallel dashed white line in the inset. (b) SEM image of other crystals from the same

batch after etching by 4 vol% HF at 295K for 20s. The schematic shows the configuration of the central component and the 90° intergrowth for the present crystal.

It was reported before that the surface structure, as observed by SEM and atomic force microscopy (AFM), of the two large faces of hourglass silicalite crystals was not identical as seen from the formation of terraces with different heights (Agger *et al.*, 2003) which is surprising if the crystal would be a perfect 90° intergrowth as proposed in Figure 3(c) which yields the same kind of crystallographic (100) surface for both large faces. Figure 4(a) shows a close-up SEM image of the side surface of the crystal in Figure 1 with the inset showing an enlarged image from the black square enclosed region. Black arrows point towards the boundary between the central matrix and the 90° intergrowth which clearly does not run perfectly along the corner of the crystal as expected for the perfect case as drawn in Figure 3(c). In an attempt to more directly observe the shape of the intergrowth boundary with SEM, some crystals were etched by 4 vol% HF at 295K for 20s. Because the arrangement of the atoms in the (100) and (010) planes is different as well as the corresponding channels in the structure, a different etching for both planes can be expected. Figure 4(b) shows a SEM image of the crystals after such an etching from which it is clear that the intergrowth does not completely cover the outside surface as would be expected from the ideal model and which is possibly related with the fact that the intergrowth components do not connect in the center of the crystal as seen above. A more realistic schematic for the present crystal (when compared with the ideal model in Figure 3(c)) is shown as an inset in Figure 4(b). Moreover, this procedure shows that the (100) surface of the crystal is more

resistant against etching than the (010) surface, possibly due to the fact that the underlying channels for the former are smaller and do not follow a straight line down into the crystal. From the inset in Figure 4(a) it is further seen that the (100) surface of 90° intergrown component is as smooth as the (100) surface of the large central matrix, as expected, while the white arrow points at some weak terrace-like contrast on the (010) surface, which is consistent with the results observed by Agger *et al.* (Agger *et al.*, 2003). In other words, due to an imperfect intergrowth, it is well possible that high magnification images from both surfaces do show different structures as they could in practice arise from different crystallographic faces.

Conclusions

The intergrowth and internal architecture of coffin-shaped ZSM-5 crystals showing optical hourglass contrast was studied by an approach combining optical microscopy, FIB and TEM. Based on STEM observations of three parallel lamellas prepared with FIB from different positions in the crystal, the 2-components model, with two pyramid-like components next to the main central component and rotated by 90° along the common c-axis, is confirmed. The pyramid-like intergrowth components reach towards each other in the middle of the crystal, but they do not connect, contrary to the idealized model. As a result, some of the sinusoidal channels in the central component are still continuous over the entire depth of the coffin, contrary to the straight channels that are affected by the 90° boundaries. A model of multi-site nucleation and growth of 90° intergrowth components is proposed. The 90° rotational intergrowth boundaries show

local zigzag features indicating a variation in growth velocity of both components, probably depending on local variations in the surrounding environment.

Acknowledgements

J.B. Lu thanks the Belgian science ministry (Belspo) for support of his post-doctoral research stay at EMAT. The work was performed in the framework of an FWO project G.0603.10N. ”Internal investigation of zeolite crystals and their guests”. We thank Maarten B. J. Roeffaers for the preparation of the ZSM-5 crystals and fruitful discussions.

References

Agger, J. R., Hanif, N., Cundy, C. S., Wade, A. P., Dennison, S., Rawlinson, P. A. & Anderson, M. W. (2003) Silicalite crystal growth investigated by atomic force microscopy. *J Am. Chem. Soc.,* **125,** 830-839.

Den Hollander, M. A., Wissink, M., Makkee, M. & Moulijn, J. A. (2002) Gasoline conversion: reactivity towards cracking with equilibrated FCC and ZSM-5 catalysts. *Appl Catal A,* **223,** 85-102.

Hay, D. G., Jaeger, H. & Wilshier, K. G. (1990) Systematic intergrowth in crystals of ZSM-5 zeolite. *Zeolites,* **10,** 571-576.

Iwasaki, A., Hirata, M., Kudo, I., Sano, T., Sugawara, S., Ito, M. & Watanabe, M. (1995) In situ measurement of crystal growth rate of zeolite. *Zeolites,* **15,** 308-314.

Iwasaki, A., Sano, T. & Kiyozumi, Y. (1998) Effect of additives on the growth behavior of silicalite crystal. *Micropor Mesopor Mat,* **25,** 119-126.

Karwacki, L., Kox, M. H. F., Matthijs de Winter, D. A., Drury, M. R., Meeldijk, J. D., Stavitski, E., Schmidt, W., Mertens, M., Cubillas, P., John, N., Chan, A., Kahn, N., Bare, S. R., Anderson, M., Kornatowski, J. & Weckhuysen, B. M. (2009) Morphology-dependent zeolite intergrowth structures leading to distinct internal and outer-surface molecular diffusion barriers. *Nat Mater,* **8,** 959-965.

Karwacki, L., Stavitski, E., Kox, M. H., Kornatowski, J. & Weckhuysen, B. M. (2007) Intergrowth structure of zeolite crystals as determined by optical and fluorescence microscopy of the template-removal process. *Angew Chem Int Ed* **46,** 7228-7231.

Klapper, H. (2010) Generation and Propagation of Defects During Crystal Growth. In: *Springer Handbook of Crystal Growth* (eds. G. Dhanaraj, K. Byrappa, V. Prasad & M. Dudley). Springer Berlin Heidelberg.

Kox, M. H. F., Stavitski, E. & Weckhuysen, B. M. (2007) Nonuniform Catalytic Behavior of Zeolite Crystals as Revealed by In Situ Optical Microspectroscopy. *Angew Chem Int Ed,* **46,** 3652-3655.

Lu, J. B., Roeffaers, M. B. J., Bartholomeeusen, E., Sels, B. F. & Schryvers, D. (2014) Intergrowth of Components and Ramps in Coffin- Shaped ZSM-5 Zeolite Crystals Unraveled by Focused Ion Beam- Assisted Transmission Electron Microscopy. *Microscopy and Microanalysis,* **20,** 42-49.

Millward, G. R., Ramdas, S., Thomas, J. M. & Barlow, M. T. (1983) Evidence for semi-regularly ordered sequences of mirror and inversion symmetry planes in ZSM-5/ZSM-11 shape-selective zeolitic catalysts. *J Chem Soc, Faraday Trans 2,* **79,** 1075.

Mueller, U. & Unger, K. K. (1988) Preliminary studies on the synthesis of alkaline-free large crystals of ZSM-5. *Zeolites,* **8,** 154-156.

Price, G. D., Pluth, J. J., Smith, J. V., Bennett, J. M. & Patton, R. L. (1982) Crystal structure of tetrapropylammonium fluoride-containing precursor to fluoride silicalite. *J Am Chem Soc,* **104,** 5971-5977.

Ristanović, Z., Hofmann, J. P., Deka, U., Schülli, T. U., Rohnke, M., Beale, A. M. & Weckhuysen, B. M. (2013) Intergrowth structure and aluminium zoning of a zeolite ZSM-5 crystal as resolved by synchrotron-based micro X-ray diffraction imaging. *Angew. Chem. Int. Ed.,* **52,** 13382-13386.

Roeffaers, M. B., Sels, B. F., Uji-i, H., Blanpain, B., L'Hoest, P., Jacobs, P. A., De Schryver, F. C., Hofkens, J. & De Vos, D. E. (2007) Space- and time-resolved visualization of acid catalysis in ZSM-5 crystals by fluorescence microscopy. *Angew Chem Int Ed,* **46,** 1706-1709.

Roeffaers, M. B. J., Ameloot, R., Baruah, M., Uji-i, H., Bulut, M., De Cremer, G., Müller, U., Jacobs, P. A., Hofkens, J., Sels, B. F. & De Vos, D. E. (2008a) Morphology of Large ZSM-5 Crystals Unraveled by Fluorescence Microscopy. *J Am Chem Soc,* **130,** 5763-5772.

Roeffaers, M. B. J., Ameloot, R., Bons, A.-J., Mortier, W., De Cremer, G., de Kloe, R., Hofkens, J., De Vos, D. E. & Sels, B. F. (2008b) Relating Pore Structure to Activity at the Subcrystal Level for ZSM-5: An Electron Backscattering Diffraction and Fluorescence Microscopy Study. *J Am Chem Soc,* **130,** 13516-13517.

Stavitski, E., Drury, M. R., de Winter, D. A. M., Kox, M. H. F. & Weckhuysen, B. M. (2008) Intergrowth Structure of Zeolite Crystals and Pore Orientation of Individual

Subunits Revealed by Electron Backscatter Diffraction/Focused Ion Beam Experiments. *Angew Chem Int Ed,* **47,** 5637-5640.

Stavitski, E., Kox, M. H. F. & Weckhuysen, B. M. (2007) Revealing Shape Selectivity and Catalytic Activity Trends Within the Pores of H-ZSM-5 Crystals by Time- and Space-Resolved Optical and Fluorescence Microspectroscopy. *Chem Eur J,* **13,** 7057-7065.

Tzoulaki, D., Heinke, L., Schmidt, W., Wilczok, U. & Karger, J. (2008) Exploring crystal morphology of nanoporous hosts from time-dependent guest profiles. *Angew Chem Int Ed,* **47,** 3954-3957.

Van der Veen, M. A., Sels, B. F., De Vos, D. E. & Verbiest, T. (2010) Localization of p-Nitroaniline Chains Inside Zeolite ZSM-5 with Second-Harmonic Generation Microscopy. *J Am Chem Soc,* **132,** 6630-6631.

Wu, X. & Anthony, R. G. (1999) Alkylation of Benzene with Formaldehyde over ZSM-5. *J Catal,* **184,** 294-297.

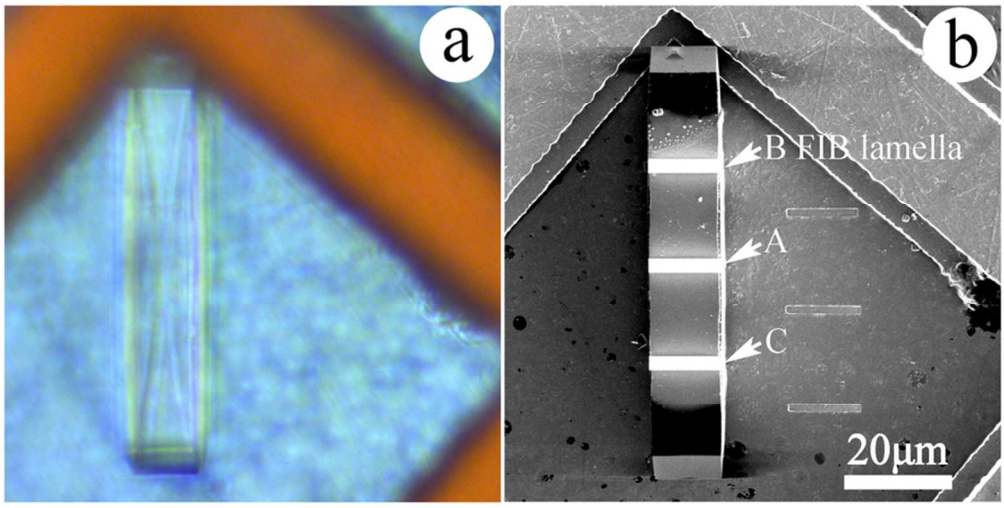

Figure 1. (a) Optical microscopy image of a coffin-shaped ZSM-5 crystal showing an hourglass pattern. (b) SEM image of the same crystal with indications of the sites for FIB sample selection.
80x40mm (300 x 300 DPI)

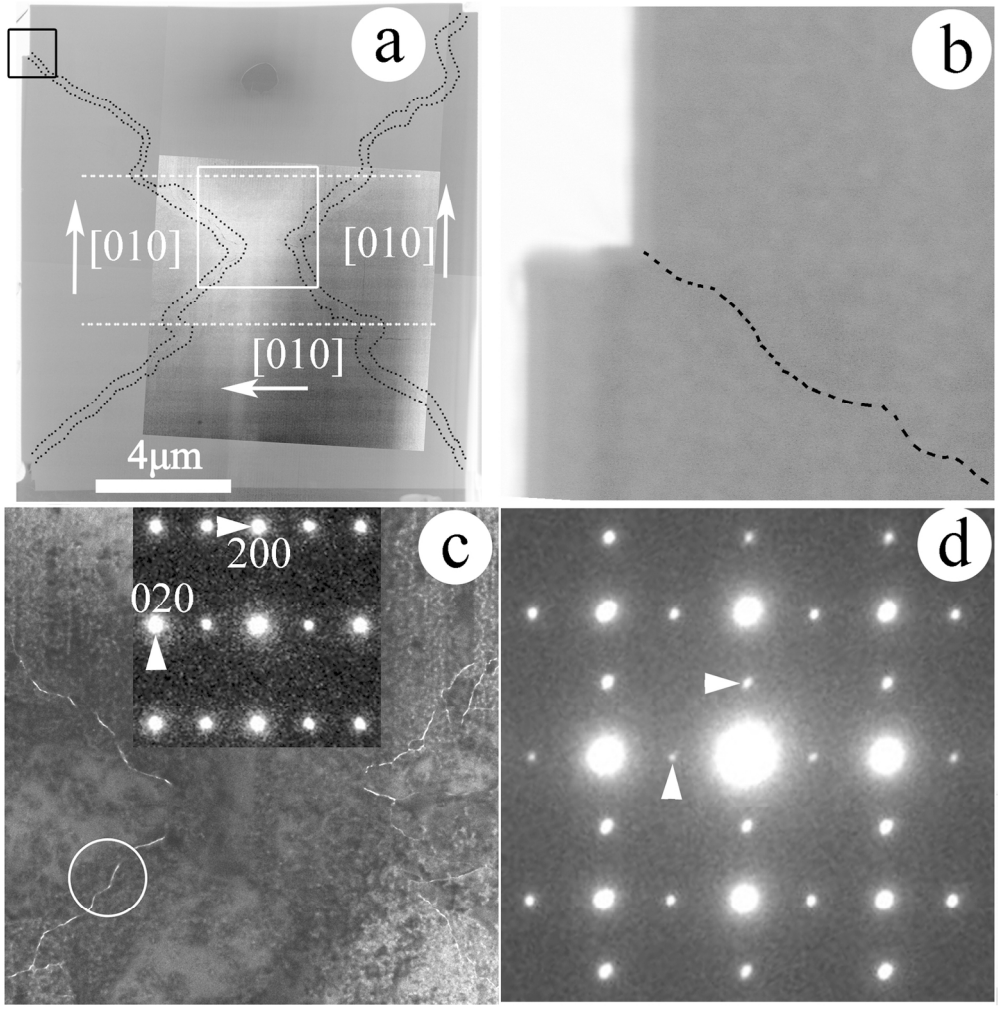

Figure 2. (a) Low magnification STEM image of lamella A. (b) Enlarged image from the black rectangle enclosed region at the upper left corner of (a). (c) Bright field (BF) image of the white square enclosed region in (a) with SAED pattern of the middle part. (d) [001] zone axis SAED pattern from the white circle enclosed boundary region in (a).
161x163mm (300 x 300 DPI)

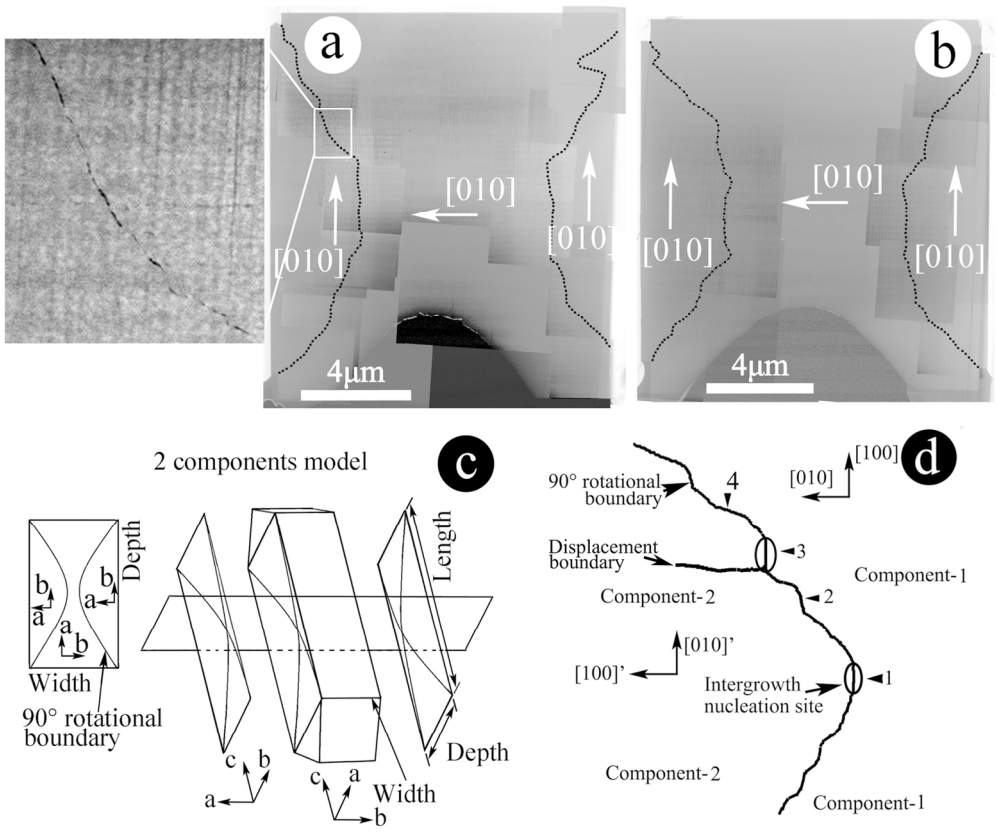

Figure 3. (a) Low magnification STEM image of lamella B. (b) Low magnification STEM image of lamella C. (c) Proposed 2-component model. (d) Proposed model of the multi-site nucleation and growth of 90° intergrowth components.
133x110mm (300 x 300 DPI)

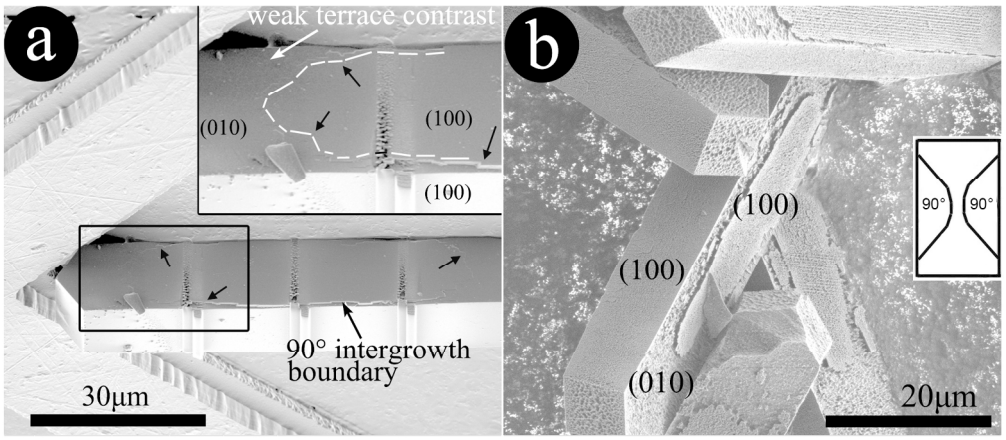

Figure 4. (a) SEM image of the side surface of the crystal in Figure 1: the boundary between the central matrix and the 90°intergrowth is indicated by black arrows and a parallel dashed white line in the inset. (b) SEM image of other crystals from the same batch after etching by 4 vol% HF at 295K for 20s. The schematic shows the configuration of the central component and the 90° intergrowth for the present crystal.
178x77mm (300 x 300 DPI)

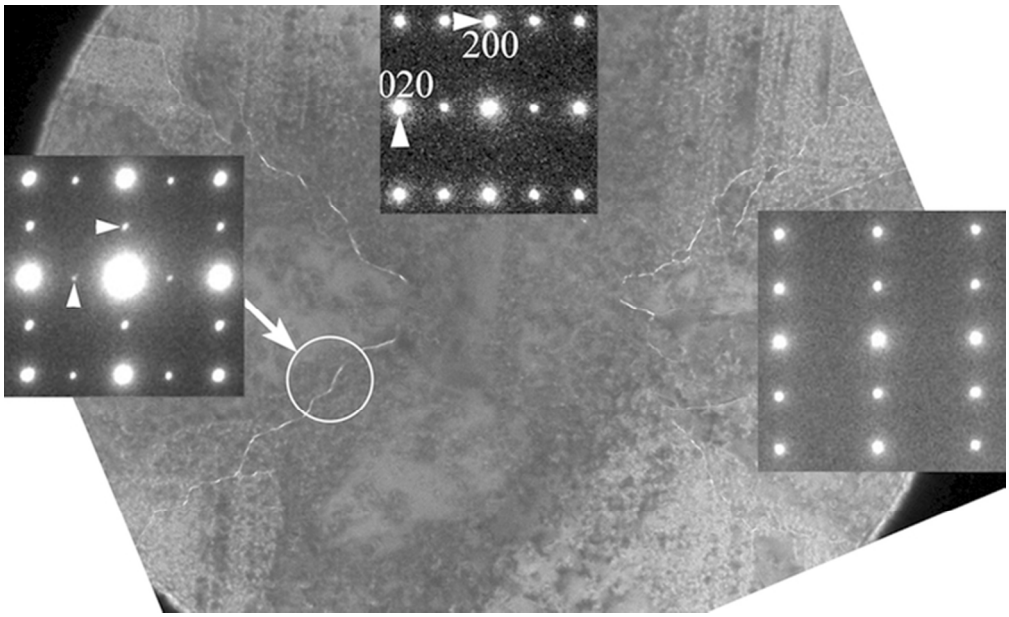

Figure S1. Bright field (BF) image of the white square indicated region in Figure 2(a). The insets represent the SAED patterns from the white circle enclosed boundary and the corresponding components from which the 90° rotational orientation relationship between the three components can be confirmed.
60x36mm (300 x 300 DPI)

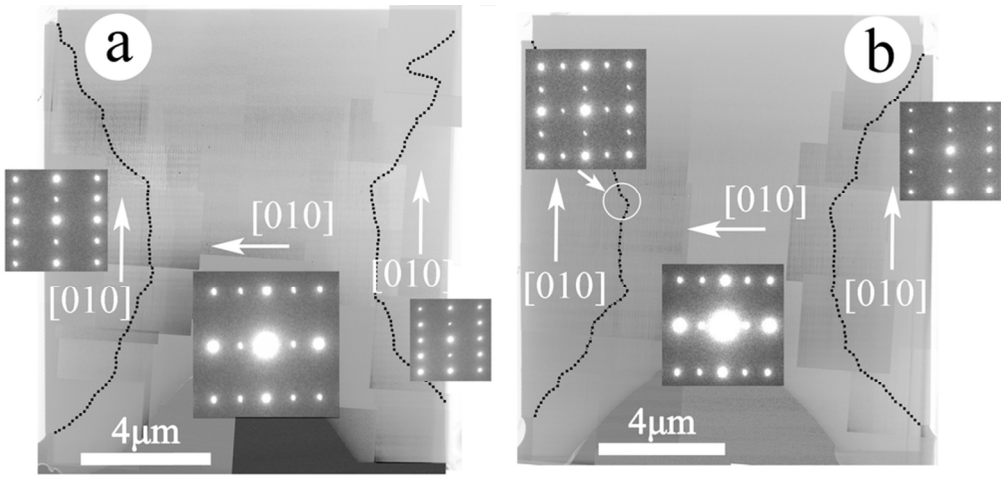

Figure S2. (a) Low magnification STEM image of lamella B. (b) Low magnification STEM image of lamella C. The insets show the SAED patterns from the corresponding components and boundary area confirming the 90° intergrowth relationship between the components.
84x40mm (300 x 300 DPI)